**Title**

Optimization of Side Shielding for Circular Positron Emission Tomographs



**Author**

Derenzo, Stephen E

**Publication Date**

1979-10-01

Lawrence Berkeley Laboratory
UNIVERSITY OF CALIFORNIA

Submitted to the Journal of Nuclear Medicine

# OPTIMIZATION OF SIDE SHIELDING FOR CIRCULAR POSITRON EMISSION TOMOGRAPHS

Stephen E. Derenzo



October 1979





Prepared for the U.S. Department of Energy under Contract W-7405-ENG-48

## DISCLAIMER

LBL-9584 Rev.

# OPTIMIZATION OF SIDE SHIELDING FOR CIRCULAR POSITRON EMISSION TOMOGRAPHS

Stephen E. Derenzo

Donner Laboratory
University of California
Berkeley, California

## ABSTRACT

This report presents expressions for the image-forming and background event rates seen by circular positron emission tomographs. These are used to determine the side shielding depth that optimizes the signal-to-noise ratio in the reconstructed image of a 20-cm cylinder of water with uniformly dispersed activity. For 1-cm wide NaI(Tl) detectors, a 50-cm patient port, an activity of 200 μCi per axial centimeter, and a shielding gap of 2 cm, the optimum shielding depth is 20 cm which results in a detector circle diameter of 90 cm. For a 25-cm patient port and other conditions as above, the optimum shielding depth is 14 cm. Optimization calculations for detector materials having different efficiency, energy resolution, and time resolution are also presented.

In positron emission transverse section tomography, the image is derived from the detection of unscattered coincident annihilation pairs. Almost all positron emission tomographs employ shielding on either side of the detectors to block activity external to the transverse section being imaged (1-7). Shielding is also used between layers in multiple section devices (8-12). In spite of this shielding, image contrast is degraded by true coincidences of scattered annihilation pairs and by accidental coincidences of unrelated annihilation photons (Fig. 1). Most positron imaging systems operate with scattered and accidental backgrounds that are each typically 20% of the detected coincidences. Even if these backgrounds can be perfectly estimated and subtracted from the detected coincidences, the statistical fluctuations in the result are greater than if the backgrounds did not exist. In the following sections we examine the trade-off between sensitivity and backgrounds and describe a procedure for determining the optimum shielding depth for circular positron emission tomographs.

## EVENT RATES

As has been shown analytically for circular positron emission tomographs (13), the overall rate of unscattered coincident events ($C_I$) is given by:

$$C_I = B_I \varepsilon^2 \rho G_e^2 / R \qquad (1)$$

where $\varepsilon$ is the detection efficiency for annihilation photons, $\rho$ is the activity density in $\mu$Ci per axial centimeter, $G_e$ is the effective shielding gap in centimeters, R is the detector ring radius in centimeters (Fig. 2), and $B_I$ is a constant that incorporates the average attenuation and numerical factors. For activity distributed in a 20-cm cylinder of water, $B_I$ = 1850. Due to edge penetration, the effective shielding gap $G_e$ is slightly larger

than the physical shielding gap G:

$$G_e = G + \delta_G \tag{2}$$

The overall rate of coincident scattered events ($C_S$) is given by (13):

$$C_S = B_S \varepsilon^2 \rho G_e^3 / (RH) \tag{3}$$

where H is the shielding depth in centimeters and $B_S$ is a constant that incorporates pulse height thresholds, the angular distribution of accepted Compton scatters and numerical factors.

The overall rate of accidental events ($C_A$) is given by (13):

$$C_A = B_A \varepsilon^2 \tau \rho^2 G_e^4 / H^2 \tag{4}$$

where $\tau$ is the full coincidence time window in nanoseconds, and $B_A$ is a constant that incorporates pulse height thresholds, detector efficiencies for scattered and unscattered photons, and numerical factors.

These rates are reduced by system deadtime, which is a combination of the deadtime of the detectors, timing and pulse height discriminators, coincidence circuits and memory. We assume that for a particular scattering medium (i.e., a 20-cm cylinder of water) the ratio of photon interactions to coincident events is fixed and an effective nonparalyzing system deadtime can be defined that applies to the total coincident event rate only. The fraction of events F that is lost to deadtime is given by:

$$F = tC_T / (1 + tC_T) \tag{5}$$

where $C_T$ is the total coincidence rate ($C_I + C_S + 2C_A$) and t is the deadtime per event. We assume that before deadtime losses the system detects $C_I + C_S + C_A$ in the on-time coincidence window and $C_A$ in an off-time window.

The observed system rates are:

$$D_I = (1-F)C_I$$
$$D_S = (1-F)C_S$$
$$D_A = (1-F)C_A \quad (6)$$

In the central region of the reconstructed image of a cylinder of activity in water, the intensity of unscattered coincident events per square centimeter ($d_I$) is given by:

$$d_I = (1-F)b_I\varepsilon^2\rho G_e^2/R. \quad (7)$$

For a 20-cm cylinder, $b_I = 29.44$. The intensity of scattered coincident events per square centimeter ($d_S$) is given by:

$$d_S = (1-F)b_S\varepsilon^2\rho G_e^3/(RH). \quad (8)$$

The intensity of accidental events per square centimeter ($d_A$) is given by:

$$d_A = (1-F)b_A\varepsilon^2\tau\rho^2 G_e^4/H^2. \quad (9)$$

Before background subtraction, the total intensity $d_T$ is given by:

$$d_T = d_I + d_S + d_A. \quad (10)$$

## FIGURE OF MERIT

A figure of merit (Q) can be defined as the product of the unscattered coincidence rate ($D_I$) and the image contrast ($d_I/d_T$) using the arguments of Beck (14):

$$Q = D_I(d_I/d_T) \quad (11)$$

Q may also be called an "effective" image event rate since the same signal-to-noise ratio would be obtained in an ideal tomograph with $D_I' = Q$ and $d_S' = d_A' = 0$. Note that $d_I$, $d_S$ and $d_A$ all undergo the same deadtime effects, attenuation correction, and error propagation in the reconstruction process. The latter results in a significant reduction in signal-to-noise and is discussed in Reference 15.

Equations 1-10 show that for a given imaging situation, reducing the shielding depth H improves the imaging rate $D_I$ but also decreases the image contrast $d_I/d_T$. Choosing a value of H that maximizes Q (Eq. 11) insures the best tradeoff between sensitivity and image contrast.

## RESULTS

NaI(Tl). The constants $\varepsilon$, $B_S$, $B_A$, $b_S$, $b_A$, and $\delta_G$ were determined for NaI(Tl) by fitting Equations 1-9 to measurements of 20-cm phantoms made by the Donner 280-crystal positron tomograph. The overall rates $D_I$, $D_S$, and $D_A$ were measured for a 20-cm diameter cylinder of activity in water (6) and $d_S/(d_S + d_I)$ and $d_A/(d_S + d_I)$ were measured at the center of reconstructed images of a 5-cm diameter cylinder containing only water surrounded by a 20-cm diameter annulus of activity in water (Fig. 2). The pulse height threshold was 100 keV, the activity was varied from 100 to 300 μCi/cm, and the shielding gap was varied from 1 to 3 cm. A good fit was obtained with $\varepsilon = 45\%$, $B_S = 5100$, $B_A = 0.73$, $b_S = 71$, $b_A = 5.3 \times 10^{-3}$, and $\delta_G = 2.1$ mm. The penetration factor $\delta_G$ was necessary in each of equations 1, 3, and 4 ($D_I$, $D_S$ and $D_A$, respectively) for an adequate fit to the data.

Table 1 lists $D_I$, $d_S/d_I$, $d_A/d_I$, $d_I/d_T$, and Q as a function of shielding depth H, for a 50-cm patient port, $\rho = 200$ μCi/cm, $G_e = 2$-cm effective shielding gap, a 20-cm diameter water cylinder, and a 1-μsec deadtime. Figure 3

presents curves of Q as a function of H for the same conditions and 25-cm and 50-cm patient ports.

Other detector materials. The relative rates $D_I$, $D_S$, and $D_A$ for bismuth germanate (BGO) detector crystals have been measured in this system with a 300-keV pulse height threshold (6), and lead to the constants $\varepsilon$ = 67%, $B_S$ = 5100, $B_A$ = 0.36, $b_S$ = 71, $b_A$ = 2.6 x $10^{-3}$. Note that the photopeak selection reduces $B_A$ and $b_A$ but not $B_S$ and $b_S$ since the scatter background consists primarily of photons above 415 keV that have scattered through $<40^{o}$ (5).

By using the efficiency, time resolution and energy resolution for other detector materials, it is possible to optimize the shielding depth for each material. Table 2 lists the results for six classes of detector materials at four activity levels. See Reference 16 for a more extensive tabulation. The detection efficiency for Ge(Li) and plastic was determined from Monte Carlo calculations that traced the interactions of a beam of 511-keV photons through a group of 1-cm wide detectors (17). The detection efficiency was defined as the fraction of incident photons that produced a signal above threshold in only one detector.

## DISCUSSION

The highest optimum value of Q is achieved with BGO at each of the four activity levels. The second best materials fall in the general class of CsF, pure NaI (cooled) and liquid xenon which have the same detection efficiency as NaI(Tl) but significantly better time resolution.

Ge(Li) is unique in having sufficient energy resolution to reject almost all tissue-scattered photons. This eliminates the coincident scattered

background and greatly reduces the accidental background. The low full-energy efficiency for 511-keV photons, however, results in low values of Q.

Plastic scintillators are unique in having such excellent timing resolution that the coincidence time window of 2 to 3 nsec is determined by the size of the patient port and the speed of light. If time resolutions of the order of ±100 psec could be realized for tomographic systems, then the timing information and the use of shorter detectors could localize the annihilation point along the line of flight to ±1.5 cm. This possibility was suggested by Anger in 1966 (18) and is used in a 3-d imaging system built by Nickels and co-workers (19). The effective sensitivity (Q) could then be improved by about a factor of 10 through reduced error propagation in the image reconstruction process (15) in spite of the shorter, less efficient detectors. As may be seen in Table 2, a tenfold increase in Q would make plastic competitive with BGO.

For the case of wire chambers with lead converters, rather optimistic values of efficiency and time resolution have been used but the resulting Quality Factors are still relatively low. The situation may improve, as several groups are investigating schemes to improve their properties (20-22).

ACKNOWLEDGEMENTS

I wish to thank T. F. Budinger, L. Carroll, and R. Huesman for helpful discussions and T. Vuletich for valuable technical assistance. This work was reported in part at the 26th Annual Meeting of the Society of Nuclear Medicine, Atlanta, Georgia, June 26-29, 1979.

This work was supported by the Division of Biomedical Research of the U.S. Department of Energy under Contract W-7405-ENG-48 and by the U.S. National Institutes of Health grant CA 17566-3.

REFERENCES

1. Robertson JS, Marr RB, Rosenblum B, et al: Thirty-two crystal positron transverse section detector. In Tomographic Imaging in Nuclear Medicine, Freedman, GS (Ed), New York, Society of Nuclear Medicine, pp 142-153, 1973

2. Hoffman EJ, Phelps ME, Mullani NA, et al: Design and performance characteristics of a whole-body positron transaxial tomograph. J Nucl Med 17: 493-502, 1976

3. Cho ZH, Cohen MB, Singh M, et al: Performance and evaluation of the circular ring transverse axial positron camera (CRTAPC). IEEE Trans Nucl Sci NS-24, No 1: 530-543, 1977

4. Bohm C, Eriksson L, Bergstrom M, et al: A computer assisted ring detector positron camera system for reconstruction tomography of the brain. IEEE Trans Nucl Sci NS-25, No 1: 624-637, 1978

5. Derenzo SE, Budinger TF, Cahoon JL, et al: High resolution computed tomography of positron emitters. IEEE Trans Nucl Sci NS-24, No 1: 544-558, 1977

6. Derenzo SE, Budinger TF, Cahoon JL, et al: The Donner 280-crystal high resolution positron tomograph. IEEE Trans Nucl Sci NS-26, No 2: 2790-2793, 1979

7. Thompson CJ, Yamamoto YL, and Meyer E: Positome II: a high-efficiency positron imaging device for dynamic brain studies. IEEE Trans Nucl Sci NS-26, No 1: 583-589, 1979

8. Brownell G, Burnham C, Correia J, et al: Transverse section imaging with the MGH positron camera. IEEE Trans Nucl Sci NS-26, No 2: 2698-2702, 1979

9. Mullani NA, Higgins CS, Hood JT, et al: PETT IV: design analysis and performance characteristics. IEEE Trans Nucl Sci NS-25, No 1: 180-183, 1978

10. Ter-Pogossain MM, Mullani NA, Hood J, et al: A multislice positron emission computed tomograph (PETT IV) yielding transverse and longitudinal images. Radiology 128: 477-484, 1978

11. Ter-Pogossian MM, Mullani NA, Hood JT, et al: Design considerations for a positron emission transverse tomograph (PETT V) for imaging of the brain. J Comput Assist Tomogr 2: 539-544, 1978

12. Carroll LR: Design and performance charcteristics of a production model positron imaging system. IEEE Trans Nucl Sci NS-25, No 1: 606-614, 1978

13. Derenzo SE, Zaklad H, and Budinger TF: Analytical study of a high-resolution positron ring detector system for transaxial reconstruction tomography. J Nucl Med 16: 1166-1173, 1975

14. Beck RN: A theory of radioisotope scanning systems. In Medical Radioisotope Scanning, vol 1, Vienna, IAEA, 1964, pp 35-56

15. Budinger TF, Derenzo SE, Greenberg WL, et al.: Quantitative potentials of dynamic emission computed tomography. J Nucl Med 19: 309-315, 1978

16. Derenzo SE: Tabulation of side shielding optimization and comparison of detector materials for circular positron emission tomographs. Berkeley, California, Lawrence Berkeley Laboratory Report LBL-9584, 1979

17. Derenzo SE: Monte Carlo calculations of the detection efficiency of linear arrays of NaI(Tl), BGO, Ge(Li) and plastic for 511 keV photons.

18. Anger HO: Survey of radioisotope camera. ISA Trans 5:311-334, 1966

19. Nickles RJ and Meyer HO: Design of a three-dimensional positron camera for nuclear medicine. Phys Med Biol 23:686-695, 1978

20. Chu D, Tam KC, Perez-Mendez V, et al: High-efficiency collimator-converters for neutral particle imaging with MWPC. IEEE Trans Nucl Sci NS-23, No 1: 634-639, 1976

21. Neumann MJ: A gas-filled channel converter for fast coincidence cameras. IEEE Trans Nucl Sci NS-24, No 1: 515-520, 1977

22. Jeavons AP, Townsend DW, Ford NL, et al: A high-resolution proportional chamber positron camera and its applications. IEEE Trans Nucl Sci NS-25, No 1: 164-173, 1978

Table 1.
SHIELDING OPTIMIZATION FOR NaI(Tl)[a]

| H<br>Shielding Depth (cm) | $D_T$<br>Observed Total[b] ($sec^{-1}$) | F<br>Deadtime Loss (%) | $D_I$<br>Image Event Rate ($sec^{-1}$) | $d_S/d_I$<br>Scatter/ Image Ratio | $d_A/d_I$<br>Accidental/ Image Ratio | $d_I/d_T$<br>Image Contrast | Q<br>Quality Factor ($sec^{-1}$) |
|---|---|---|---|---|---|---|---|
| 5 | 118,582 | 11.9 | 8,805 | 0.97 | 2.59 | 0.22 | 1,932 |
| 10 | 40,000 | 4.0 | 8,220 | 0.48 | 0.76 | 0.45 | 3,672 |
| 15 | 22,350 | 2.2 | 7,325 | 0.32 | 0.38 | 0.59 | 4,295 |
| 20[c] | 15,352 | 1.5 | 6,558 | 0.24 | 0.24 | 0.67 | 4,418 |
| 25 | 11,718 | 1.2 | 5,924 | 0.19 | 0.17 | 0.73 | 4,337 |
| 30 | 9,513 | 1.0 | 5,397 | 0.16 | 0.13 | 0.77 | 4,175 |
| 40 | 6,971 | 0.7 | 4,579 | 0.12 | 0.09 | 0.83 | 3,789 |
| 50 | 5,541 | 0.6 | 3,974 | 0.10 | 0.06 | 0.86 | 3,422 |
| 60 | 4,617 | 0.5 | 3,510 | 0.08 | 0.05 | 0.88 | 3,102 |

[a] port = 50 cm, effective shielding gap $G_e$ = 2 cm, pulse height threshold = 100 keV, detector efficiency $\varepsilon$ = 45%, $\rho$ = 200 μCi/cm, deadtime t = 1 μsec, coincidence time window $\tau$ = 15 nsec.

[b] Total rate in on-time and off-time coincidence windows combined.

[c] H = 19.8 cm for maximum Q.

Table 2.
OPTIMUM VALUES OF H AND Q FOR VARIOUS DETECTOR MATERIALS[a]

| | NaI(Tl) | BGO | CsF<br>NaI (cooled)<br>Liquid Xe | Ge(Li) | Wire Chambers | Plastic |
|---|---|---|---|---|---|---|
| pulse height threshold | 100 keV | 300 keV | 100 keV | 505 keV | 200 keV | 100 keV |
| 511 keV efficiency: $\varepsilon$ | 45%[b] | 67%[b] | 45%[b] | 15%[b] | 20% | 20%[b] |
| Coincidence time window: $\tau$ | 15 ns | 30 ns | 3.3 ns | 15 ns | 50 ns | 3.3 ns |
| $B_S$ | 5,100 | 5,100 | 5,100 | 0 | 5,100 | 5,100 |
| $B_A$ | 0.73 | 0.36 | 0.73 | 0.15 | 0.50 | 0.73 |
| $b_S$ | 71 | 71 | 71 | 0 | 71 | 71 |
| $b_A$ | $5.3\times10^{-3}$ | $2.6\times10^{-3}$ | $5.3\times10^{-3}$ | $1.0\times10^{-3}$ | $3.5\times10^{-3}$ | $5.3\times10^{-3}$ |
| $\rho$ = 100 μCi/cm | | | | | | |
| Shielding depth: H (cm) | 16.3 | 16.5 | 12.7 | 6.9 | 19.8 | 12.5 |
| Image contrast: $d_I/d_T$ | 0.68 | 0.69 | 0.70 | 0.88 | 0.66 | 0.69 |
| Quality factor: Q ($sec^{-1}$) | 2,460 | 5,417 | 2,750 | 459 | 435 | 546 |
| $\rho$ = 200 μCi/cm | | | | | | |
| Shielding depth: H (cm) | 19.8 | 20.3 | 14.1 | 8.9 | 24.7 | 13.8 |
| Image contrast: $d_I/d_T$ | 0.67 | 0.68 | 0.70 | 0.85 | 0.63 | 0.69 |
| Quality factor: Q ($sec^{-1}$) | 4,419 | 9,648 | 5,263 | 835 | 750 | 1,051 |
| $\rho$ = 500 μCi/cm | | | | | | |
| Shielding depth: H (cm) | 27.6 | 29.4 | 17.6 | 12.5 | 34.6 | 16.7 |
| Image contrast: $d_I/d_T$ | 0.65 | 0.67 | 0.69 | 0.80 | 0.58 | 0.68 |
| Quality factor: Q ($sec^{-1}$) | 8,846 | 18,858 | 11,799 | 1,775 | 1,421 | 2,399 |
| $\rho$ = 1000 μCi/cm | | | | | | |
| Shielding depth: H (cm) | 37.9 | 42.1 | 22.4 | 16.4 | 46.4 | 20.4 |
| Image contrast: $d_I/d_T$ | 0.63 | 0.66 | 0.69 | 0.76 | 0.53 | 0.67 |
| Quality factor: Q ($sec^{-1}$) | 13,827 | 28,561 | 20,473 | 3,031 | 2,149 | 4,284 |

[a]Port = 50 cm, effective shielding gap $G_e$ = 2 cm, deadtime t = 1 μsec per coincident event

[b]Detector size 1 cm wide x 5 cm deep

## FIGURE CAPTIONS

FIG. 1. Coincident event types detected by positron tomographs. The image is formed from unscattered coincident annihilation pairs. Coincident scattered pairs and accidental coincidences of unrelated photons result in a broad background.

FIG. 2. Detector, shielding, and phantom geometry for optimization calculations. Scatter background can be measured in the inner cylinder by imaging with activity in the outer cylindrical annulus only.

FIG. 3. Effective event rate Q as a function of shielding depth for NaI(Tl) detectors with 45% detection efficiency, a 2-cm shielding gap, 200 μCi/cm, 1-μsec deadtime, and a coincidence resolving time of 15 nsec. Optimum values are indicated with arrows for 25- and 50-cm patient ports.

## FATES OF ANNIHILATION PHOTONS

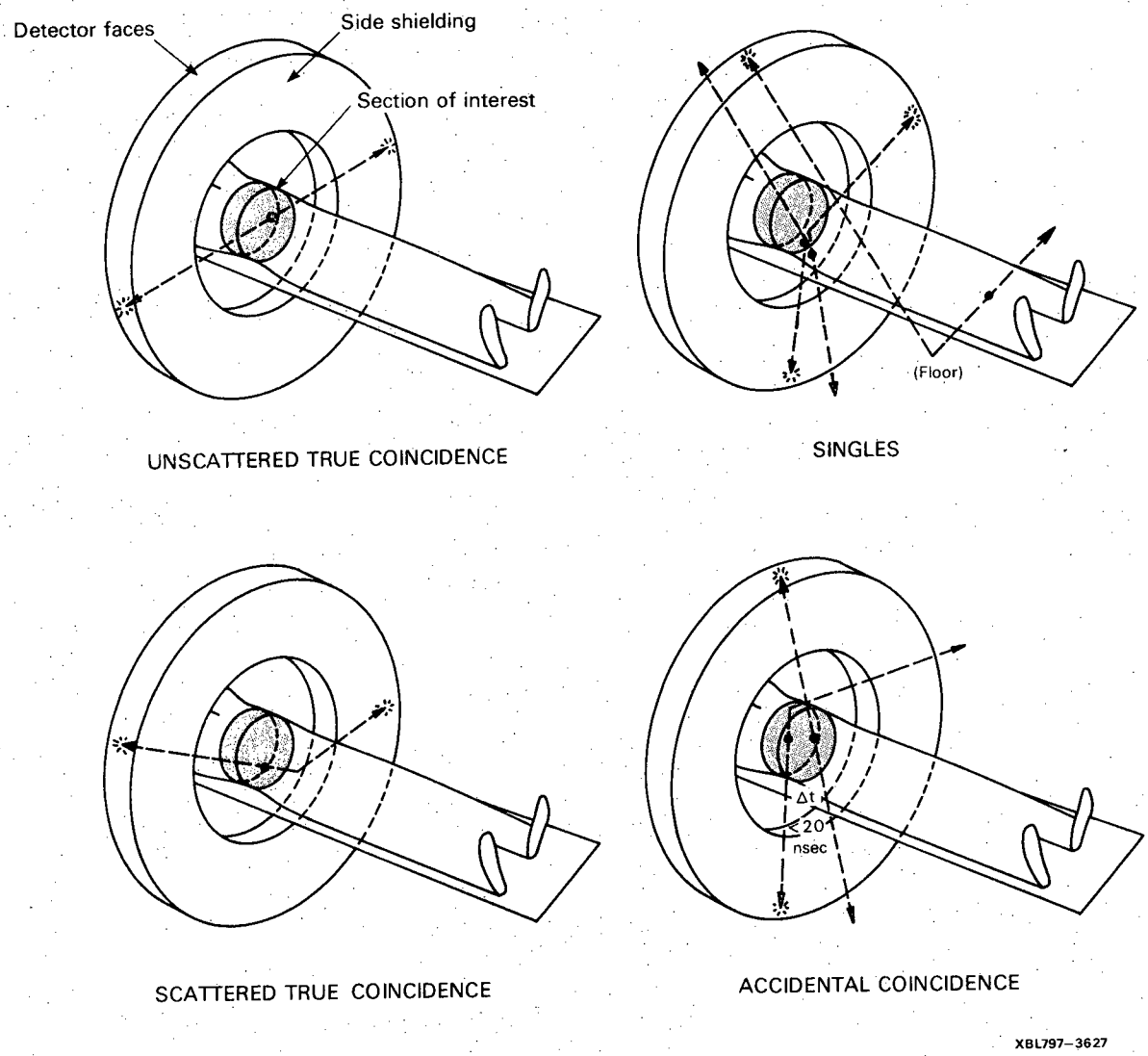


UNSCATTERED TRUE COINCIDENCE

SINGLES

SCATTERED TRUE COINCIDENCE

ACCIDENTAL COINCIDENCE

XBL797-3627

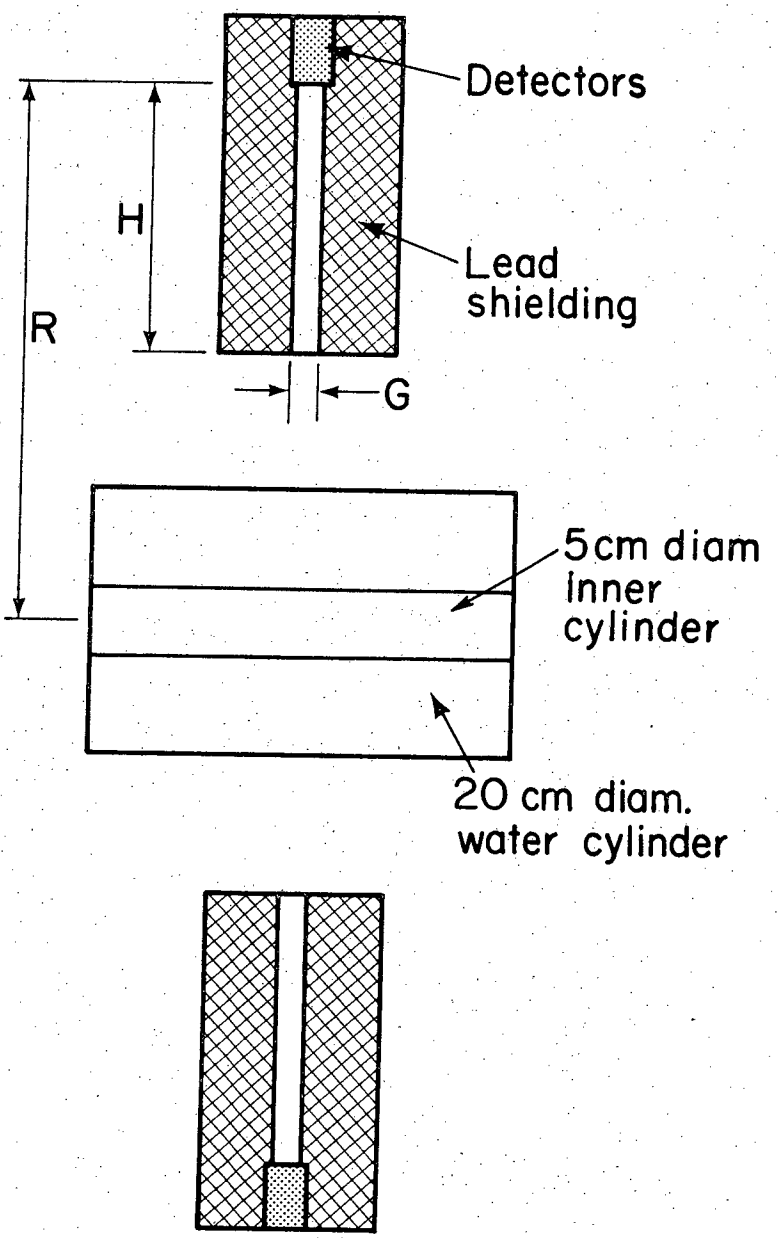
Detectors
H
R
Lead
shielding
G
5cm diam
inner
cylinder
20 cm diam.
water cylinder

XBL797-3625

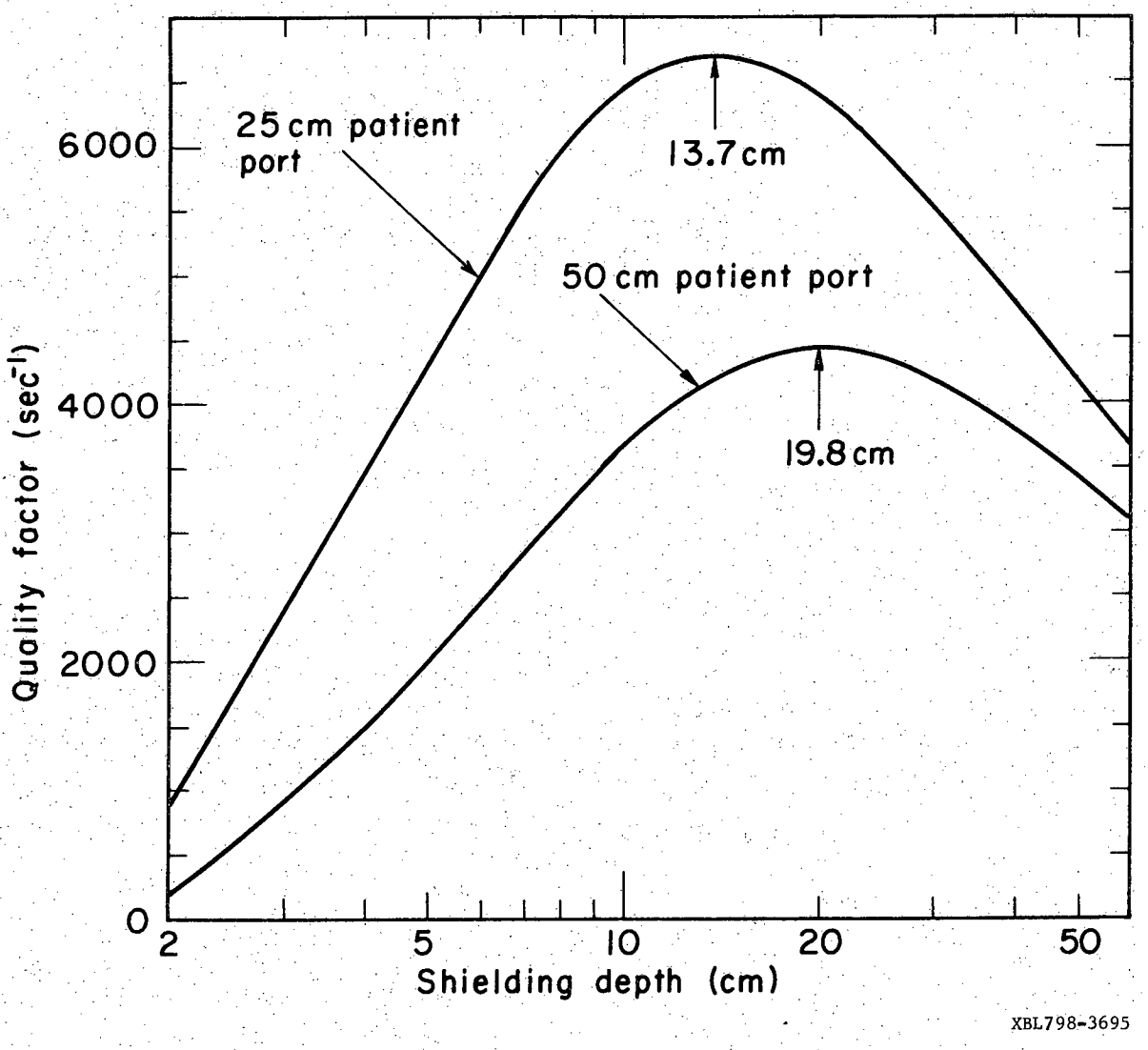
25 cm patient port
13.7 cm
50 cm patient port
19.8 cm
6000
4000
2000
0
Quality factor (sec⁻¹)
2
5
10
20
50
Shielding depth (cm)

XBL798-3695

This report was done with support from the Department of Energy. Any conclusions or opinions expressed in this report represent solely those of the author(s) and not necessarily those of The Regents of the University of California, the Lawrence Berkeley Laboratory or the Department of Energy.

Reference to a company or product name does not imply approval or recommendation of the product by the University of California or the U.S. Department of Energy to the exclusion of others that may be suitable.

*TECHNICAL INFORMATION DEPARTMENT*
*LAWRENCE BERKELEY LABORATORY*
*UNIVERSITY OF CALIFORNIA*
*BERKELEY, CALIFORNIA 94720*